



Defect reduction by liquid phase epitaxy of germanium on single-crystalline-like germanium templates on flexible, low-cost metal substrates

Journal:	<i>CrystEngComm</i>
Manuscript ID	CE-ART-07-2018-001258.R1
Article Type:	Paper
Date Submitted by the Author:	13-Sep-2018
Complete List of Authors:	<p>Li, Yongkuan; University of Houston, Mechanical Engineering Guo, Haichao; University of Houston yao, yao; University of Houston, Mechanical Engineering; Texas Center for Superconductivity and Advanced Manufacturing Institute Dutta, Pavel; University of Houston, Mechanical Engineering; UH Energy Research Park, Rathi, Monika; University of Houston, Mechanical Engineering Zheng, Nan; South Dakota School of Mines and Technology, Nanoscience and Nanoengineering Gao, Ying; University of Houston, Mechanical Engineering Sun, Sicong; University of Houston, Mechanical Engineering Ryou, Jae-Hyun; University of Houston, Mechanical Engineering Ahrenkiel, Phil; South Dakota School of Mines & Technology, Nanoscience and Nanoengineering Ph.D. Program Selvamanickam, Venkat; University of Houston, Mechanical Engineering; University of Houston, Texas Center for Superconductivity</p>



Journal Name

ARTICLE

Defect reduction by liquid phase epitaxy of germanium on single-crystalline-like germanium templates on flexible, low-cost metal substrates

Received 00th January 20xx,
Accepted 00th January 20xx

DOI: 10.1039/x0xx00000x

www.rsc.org/

Yongkuan Li^{a*}, Haichao Guo^a, Yao Yao^a, Pavel Dutta^a, Monika Rathi^a, Nan Zheng^b, Ying Gao^a, Sicong Sun^a, Jae-Hyun Ryou^a, Phil Ahrenkiel^b, and Venkat Selvamanickam^a

Single-crystalline-like Germanium (Ge) templates were demonstrated on low-cost, flexible metal substrates and have been used to fabricate III-V materials and devices for photovoltaics and flexible electronics applications. However, these Ge templates, fabricated by magnetron sputtering or plasma enhanced chemical vapor deposition, contain a high density of defects. In order to improve the performance of optoelectronic devices made using the Ge templates, a homo-epitaxial Ge layer has been additionally grown by a liquid phase epitaxy (LPE) method. The LPE Ge layer is composed of significantly larger grains (~26 μm) compared to that of the Ge template (~200 nm). This large size of the LPE Ge grains effectively reduces the volume fraction of grain boundaries. The LPE Ge shows an out-of-plane texture $\Delta\omega$ of $\sim 0.63^\circ$ and an in-plane texture $\Delta\phi$ of $\sim 1.26^\circ$, which signify improvements of $\sim 39.3\%$ and $\sim 76.6\%$ compared to that of the vapor-deposited Ge template, respectively. Further, the LPE Ge is strain free, compared to the strained Ge template hetero-epitaxially grown on Cerium Oxide. Defects caused by low-angle grain boundaries, impurities and strain relaxation in the Ge template are found to be suppressed in the LPE Ge. The threading dislocation density is roughly estimated to be $\sim 5 \times 10^6 \text{ cm}^{-2}$ in the LPE Ge compared to $\sim 1 \times 10^{10} \text{ cm}^{-2}$ in the Ge template.

1 Introduction

Germanium (Ge) was used to fabricate point contact diodes¹, transistors², high-resolution gamma-ray detectors³, and far-infrared detectors⁴ etc., in the early stage of the semiconductor history. Then, even though the mobility of bulk Ge is much higher than that of bulk silicon, Ge was replaced by Si in electronic devices^{5,6}. Compared to Ge, silicon offers the benefits of a larger bandgap for higher temperature operation, a low leakage current, and a stable oxide which performs well as a passivation layer and for lithography. However, Ge may regain its popularity owing to recent innovations, which include the development of germanium oxynitride as a mask material for Ge devices⁷, and the tuning of its band gap by band-structure engineering⁸. Furthermore, Ge-based new

concepts of materials and devices have been ongoing^{9,10}. However, the cost of these devices is high due to the expense of high-quality Ge wafers^{11,12}. In order to take advantage of the high mobility of Ge, especially its hole mobility which is the highest among all known semiconductors⁹, high-quality Ge with low defect density should be produced cost-effectively.

We had previously demonstrated a low-cost and flexible single-crystalline-like Germanium (Ge) template on flexible metal substrates based on the Ion Beam Assisted Deposition (IBAD) technique¹³, for use in high-performance Si flexible electronics^{14,15} and GaAs solar cells¹⁶. The Ge template exhibits a strong biaxial texture with a spread in the out-of-plane texture ($\Delta\omega$) and a spread in the in-plane texture ($\Delta\phi$) as small as $\sim 1.1^\circ$ and $\sim 3.1^\circ$, respectively¹⁶. Still the high density of grain boundaries in these films consisting of small grains (~ 200 nm) can act as recombination centers and limit the device performance. The motivation of this work is to transform the single-crystalline-like Ge templates to a much larger grain size with fewer defects. Large grain size (30–60 μm) Ge templates were previously reported using large-grained metal substrate based on rolling-assisted biaxially textured substrates (RABiTS)¹⁷, but such Ge exhibited an inferior texture with $\Delta\omega$ of $\sim 6.8^\circ$ and $\Delta\phi$ of $\sim 6.5^\circ$, and small Ge grains may still exist

^a Department of Mechanical Engineering & Texas Center for Superconductivity and Advanced Manufacturing Institute, University of Houston, Houston, TX 77204, USA.

^b Nanoscience and Nanoengineering, South Dakota School of Mines and Technology, Rapid City, SD 57701, USA

† corresponding author: yli78@uh.edu.

Electronic Supplementary Information (ESI) available: [Boat design; Proof of (111) facets; Proof of epitaxy of LPE Ge layer over Ge (111) wafer]. See DOI: 10.1039/x0xx00000x

within the “large grains” with proof of only optical microscope images.

In this work, we employed liquid phase epitaxy (LPE) to fabricate a homo-epitaxial Ge layer on the Ge template. This growth method could be used to fabricate high purity¹⁸ and high quality¹⁹ materials under quasi-equilibrium conditions, in comparison to gas-phase methods like physical vapor deposition (PVD) and chemical vapor deposition (CVD). Besides, LPE offers a high growth rate²⁰ which is beneficial for both large grain growth and low-cost mass production. The evidence and the discussion on how the LPE method functions in terms of defect reduction and texture improvement will be provided in this manuscript.

2 Experimental

Single-crystalline-like Ge templates were grown epitaxially in a reel-to-reel magnetron sputtering system on IBAD-buffered flexible Hastelloy tapes and the buffer layers include a cerium oxide (CeO₂) film¹³. LPE Ge was then deposited on top of the flexible Ge template using a horizontal slide boat system. Ge (001) and Ge (111) wafers were also used as substrates for LPE Ge growth. A quartz tube in a Lindberg 3-zone furnace (model: 55667) was used as the reactor. A sliding graphite boat with 4 source wells suitable for multi-layer deposition, and a K-type thermocouple inserted in the slider were used. Four caterpillar wells beside the source wells were utilized to reduce the residue solution after growth. Shims with different thickness are also used to reduce the residue

amount as much as possible. (details of the boat design is shown in Figure S1 in supporting materials)

Lead (Pb) was used as the solvent. According to the lead-germanium phase diagram²¹, a 3 at. % Ge precursor was selected, with 0.14g Ge in each run. Commercially-purchased Ge pieces and lead shots with purities of 99.999% and 99.99%, respectively, were used. The substrates were ultrasonically cleaned in a bath of isopropyl alcohol for 10 minutes at room temperature, and then blow dried with N₂. After installing the substrate onto a shim, it was placed under the well beside the source well in the boat. The system was then pumped down with a rough pump to around 2 mTorr and then, 70 sccm forming gas containing 2.9 a.t. % hydrogen mixed with Argon were introduced into the quartz reactor. Three cycles of purging were carried out to reduce residual O₂ in the reactor. The source was heated to 670°C and soaked for 1 hour to homogenize the liquid phase precursor and break down the Ge surface oxides. The temperature was then decreased to the contact temperature (T_c) and held for 12minutes, during which the substrate was pulled into the source well for growth by a stepper motor. The cooling rate was set to 60°C/h for the LPE deposition, after which the substrate was pulled away from the source well at the end growth Temperature (T_e). The growth range was varied to achieve different sizes and densities of the Ge grains as listed in Table I. After cooling the sample down in the furnace to room temperature, Pb residue was etched away quickly (typically in 30 seconds) to avoid the etching of Ge, by a mixture of water, hydrochloric acid, and hydrogen peroxide with a volume ratio of 1:1:1 at 65 °C.

Table I LPE samples grown at different growth ranges on different substrates and the corresponding average grain size and average grain density statistically estimated from SEM images.

Sample	<i>a</i>	<i>b</i>	<i>c</i>	<i>d</i>	<i>e</i>	<i>f</i>
Substrate	Flexible Ge (001) template	Ge (001) wafer	Ge (111) wafer			
Growth range T _c - T _e (°C)	600-595	600-590	600-550	600-500	600-550	600-550
Average grain size (μm)	19	20	26	34		
Average grain density (/0.04mm ²)	93	72	43	37		

Scanning electron microscopy (SEM) images of the LPE samples were collected using a JEOL JSM-6330F, and the substrate SEM image was collected with a LEO 1525. A triple-axis high-resolution X-ray diffraction (HRXRD) machine (Bruker D8) was used to study the crystalline quality of the Ge layer, employing θ -2 θ scans and rocking curves. Besides, pole figures were measured with a 2D General Area Detector Diffraction (GADDS) System, and ϕ -scan patterns were derived by integrating the pole figures along the χ angle. Transmission electron microscope (TEM) images were obtained with a JEOL 2000FX. High resolution Transmission electron microscope (HRTEM) images were collected with JEOL JEM-2010. Cross section TEM samples were prepared with an FEI 235 focused ion beam (FIB) milling system.

3. Results and discussion

3.1 Growth mechanism

In the following text, unless otherwise specified, the substrate Ge stands for the flexible thin film single-crystalline-like Ge template on metal substrate¹³. The SEM images of the substrate Ge, and samples *c*, *e* and *f* are displayed in Figure 1. The substrate Ge shown in Figure 1 (a) consists of uniformly distributed grains with an average size of ~200 nm. Much larger Ge grains are found in the LPE Ge grown on this substrate. The LPE Ge of sample *c* shown in Figure 1 (b) has an average size of ~26 μm, which is over two magnitudes larger than that of the Ge substrate. The significantly-increased grain size is the motivation to employ LPE to reduce the volume fraction of grain boundaries.

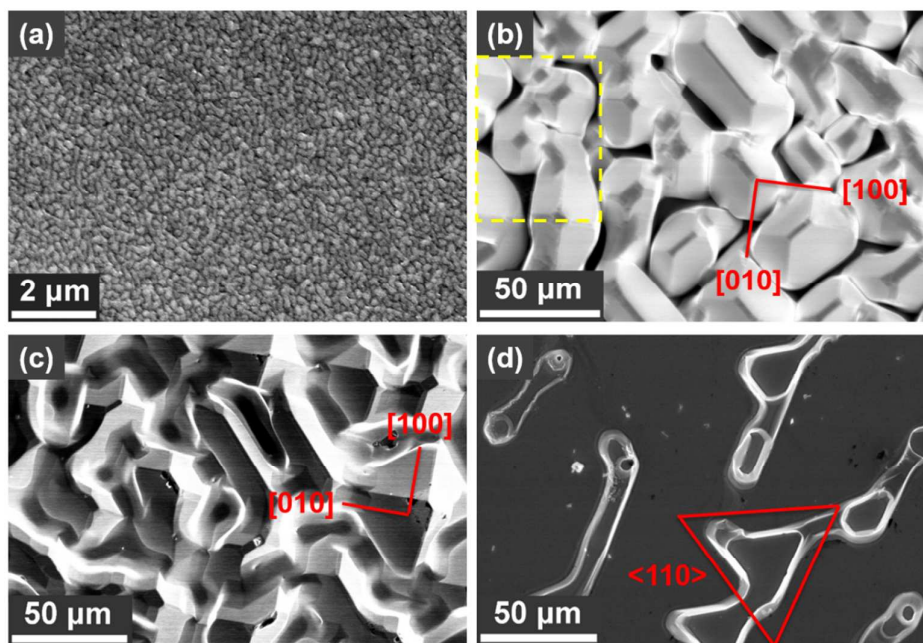


Figure 1 SEM images of (a) the substrate Ge template, (b) the LPE Ge layer grown on the substrate Ge (sample c), the LPE layer grown on (c) a Ge (001) wafer (sample e) and (d) a Ge (111) wafer (sample f). The probable crystal directions are marked in red.

While details of the crystal quality will be described in Sections 3.2 and 3.3, we find from Figure 1 (b) that the LPE Ge grains are faceted, suggesting high crystallinity. Furthermore, the grains are pyramid-like, strongly indicating island growth. The facets are identified as four {111} surfaces, which intersect the base (001) surface along $\langle 110 \rangle$ directions. The evidence for the identification of {111} facets is found in the cross-sectional SEM image (Figure S2 in supporting materials), with the angle between the facets and the base surface of around 54.7° . With this knowledge, the alignment of the grains into a single-crystalline-like layer is clearly shown in Figure 1(b). Additionally, some of the grains are truncated, with top and corner facets as probably {001} surfaces. A similar pyramidal structure is found in sample *e* on a Ge (001) wafer as shown in Figure 1 (c). Compared to sample *e*, sample *c* is porous probably due to the misorientation between the grains. Nevertheless, each LPE grain of sample *c* is large enough as a seed for various kinds of micro- and nano- scale devices based on Ge, Si, or GaAs, while the negative effects of the pores could be avoided through careful fabrication and integration. Further, micro-scale pyramid-like structure has been reported to be beneficial for light-trapping in bulk crystalline Si²², Si thin film²³ and non-Si thin film solar cells²⁴, yielding a higher External Quantum Efficiency (EQE). Besides, the pyramids provide an extra benefit by converting the (001)-oriented Ge into a pseudo-(111)-oriented Ge, that could make it possible to epitaxially grow hexagonal materials on them. A flat surface can also be achieved with further polishing of the LPE layer.

An obvious different surface structure is found in the LPE Ge layer of sample *f* on a Ge (111) wafer shown in Figure 1(d). Instead of the pyramidal shapes, it has a flat surface with hexagonal or triangular areas enclosed by possibly growth

steps. These growth steps are reasonably supposed to be along $\langle 110 \rangle$ directions, resulting from the epitaxy of LPE Ge (111) layer over the Ge (111) wafer (shown in Figure S3 and Figure S4 in supporting materials for additional evidence of the epitaxy of the LPE (111) layer). The contrast of surface morphology of LPE on Ge substrates with different orientations could be explained by the lower surface energy of the Ge (111) plane than that of the Ge (001) plane, which are reported²⁵ to be 1.30 J/m^2 and 1.71 J/m^2 , respectively. Since the LPE process is quasi-equilibrium, the growth along the $\langle 001 \rangle$ directions is faster than that along the $\langle 111 \rangle$ directions, resulting in a 3-dimension (3D) growth with both laterally and normally fast propagating surfaces, leaving (111) facets exposed in samples *c* and *e*. The truncated pyramidal shape is another indication of the 3D growth mechanism. According to this growth mechanism, a basic model of the LPE Ge structure is proposed in Section 3.4 to explain the texture improvement and the defect reduction.

3.2 Texture improvement

(In the following text, unless otherwise stated, the LPE Ge stands for sample *c*.) The biaxial texture of the substrate Ge and the LPE Ge are demonstrated in Figure 2. As shown in the θ - 2θ scans in Figure 2 (a), only one peak can be assigned to Ge before and after the LPE Ge growth; while in the ϕ scans in Figure 2 (c), an obvious four-fold symmetry is observed in both samples. Further, to study the quality of the LPE Ge, $\Delta\omega$ and $\Delta\phi$ are derived by fitting the ω peaks (Figure 2 (b)) and the ϕ peaks (Figure 2 (c)) respectively to a Gaussian function. The average full-width-at-half-maximum (FWHM) of the four ϕ -scan peaks was calculated to determine $\Delta\phi$, while the FWHM of the ω peak represents $\Delta\omega$. As listed in Table II, $\Delta\omega$ and $\Delta\phi$ of

the LPE Ge are found to be $\sim 0.63^\circ$ and $\sim 1.26^\circ$, which are $\sim 39.3\%$ and $\sim 76.6\%$, respectively, less than those of the substrate Ge. This significant improvement in texture can effectively reduce the misorientation along the grain boundaries. Along with the reduced volume fraction of grain

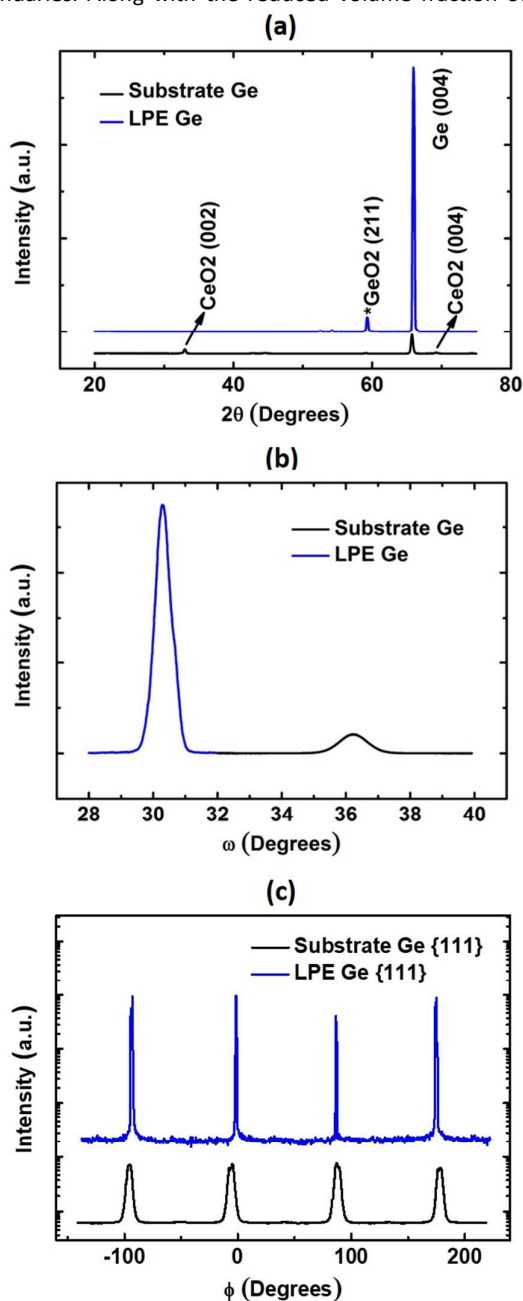


Figure 2 HRXRD scans of the flexible substrate Ge and the LPE Ge (sample c): (a) θ - 2θ scans; (b) ω scans of the Ge (004) peaks; (c) ϕ scans of the Ge {111} peaks. The substrate Ge is grown on a buffer of CeO_2 , peaks of which are identified in (a). The peak at around 59° is tentatively identified as a GeO_2 (211) peak, caused by surface oxidation or oxygen diffusion from the CeO_2 layer.

boundaries by the large grain size, high-quality Ge is achieved, as will be shown in section 3.3.

Further, as presented in Figure 2, XRD intensity in all scans of the LPE Ge are drastically enhanced compared to the substrate Ge, resulting from the large size of LPE grains. After fitting the Ge (004) peaks in Figure 2 (1) to a Gaussian function, the peak positions are derived to be 65.98° and 65.74° for the LPE Ge and the substrate Ge, respectively. Comparing to the standard Ge (004) position of powder samples which is 66.02° (ICDD card. 00-004-0545), an obvious left shift is found for the peak position of the substrate Ge. This left shift suggests a strained Ge lattice with a larger lattice constant along the c -axis which is caused by the lattice mismatch between Ge and the underlying CeO_2 . Relaxation of strain could be one of the defect sources in single-crystalline-like Ge. Since the Ge (004) peak of the LPE Ge is essentially at the standard position, it is likely free of strains and in turn has fewer defects.

Table II. $\Delta\omega$ and $\Delta\phi$ values derived from the HRXRD ω scans (Figure 2 (b)) and the ϕ scans (Figure 2 (c)) for both the substrate Ge and the LPE Ge (sample c). The values of a commercial Ge (001) wafer measured using the same method are listed as indicators of instrumental broadening.

Sample	$\Delta\omega$	$\Delta\phi$
Substrate Ge	$\sim 1.04^\circ$	$\sim 5.41^\circ$
LPE Ge (sample c)	$\sim 0.63^\circ$	$\sim 1.26^\circ$
Ge wafer	$\sim 0.56^\circ$	$\sim 0.91^\circ$

3.3 Defect reduction

Cross-section (CS) TEM and High Resolution TEM (HRTEM) images are obtained to determine the quality of the Ge samples, and the images are displayed in Figure 3. The substrate Ge is seen to be very defective in the dark field (DF) TEM image in Figure 3 (c). In contrast, the DF TEM image of the LPE Ge shown in Figure 3 (a) is much cleaner. The overall defect density of the LPE Ge is roughly estimated to be around $5 \times 10^6 \text{ cm}^{-2}$ from Figure 3 (a), which is more than three orders of magnitude lower than the defect density of the substrate Ge (higher than $1 \times 10^{10} \text{ cm}^{-2}$). Device-quality Ge is achieved by the LPE method with defect density comparable to Ge used for high-performance photodetectors²⁶.

A closer examination of Figure 3 (a) reveals several threading dislocation cores as marked. Many more defects are observed in Figure 3 (c) in the substrate Ge film, including twins, stacking faults and threading dislocations. HRTEM images shown in Figure 3 (b) and (d) display a dislocation core of the LPE Ge and planar defects in the substrate Ge, respectively. Besides, the Fourier transformation pattern suggests that the LPE Ge is a single crystal as shown in the inset of Figure 3 (b), while extra spots are found beyond the single crystal pattern in the inset of Figure 3 (d), caused by defects in the substrate Ge.

3.4 Discussion

The microstructure of LPE Ge in sample c is supposed to have developed by the following process. Scattered LPE grains are initially formed on the substrate Ge in an island growth mode as mentioned in Section 3.1. With further growth, the

grains impinge each other, and grain boundaries are formed. By increasing the growth range with the same T_c in samples *a*, *b*, *c* and *d*, the grain density decreases as shown in Table 1, implying that the grains grow competitively after the impingement. Hence, only some of the grains grow further, covering their neighbors, shown in the dashed box in Figure 1 (b). Then the LPE Ge layer of sample *c* consists of the following: small LPE grains on many tiny substrate Ge grains, and large LPE grains on several small LPE grains. Basic models of the

defect density of the LPE Ge. In case of films grown by hetero-epitaxy, the threading dislocation density caused by strain relaxation is reported to be proportional to the inverse of the film thickness²⁸. Assuming that the LPE layer thickness is the average LPE grain height which is $\sim 18 \mu\text{m}$, the LPE Ge is only around twenty times thicker than the substrate Ge ($\sim 0.8 \mu\text{m}$). So, additional sources of defects are likely curbed by the LPE Ge over the substrate Ge.

Two additional sources of defects in the substrate Ge are

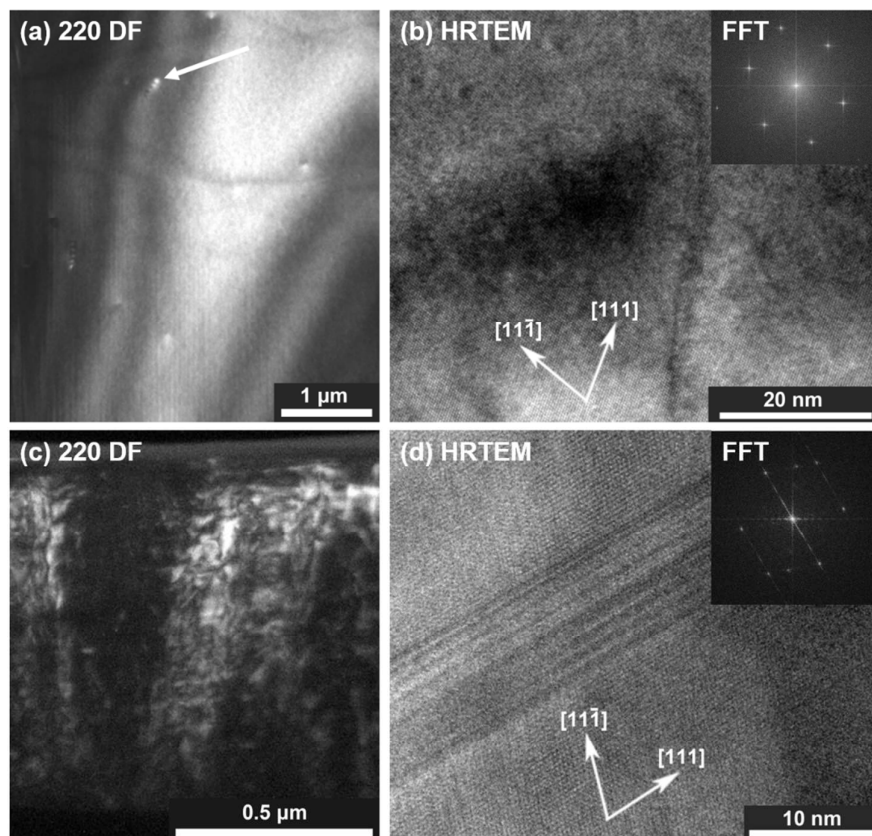


Figure 3 Dark-field (DF) cross-section TEM images of (a) the LPE Ge (sample *c*) and (c) the substrate Ge with zone axis of [220]; Bright field HRTEM images of (b) the LPE Ge and (d) the substrate Ge with zone axis of [220], with insets showing the corresponding Fourier transformation (FFT) patterns.

small and large LPE grains are displayed in Figure 4.

The texture improvement of the LPE Ge can be mainly accounted for by the unique structure of the LPE grains illustrated in Figure 4. Through an orientation averaging mechanism²⁷, the large and small LPE grains likely have averaged the random mis-orientations of the tiny substrate Ge grains. Therefore, $\Delta\omega$ and $\Delta\phi$ of sample *c* are reduced by 39.3% and 76.6%, respectively, compared to the substrate Ge.

The LPE Ge of sample *c* shows a significantly reduced defect density, which is roughly three magnitudes lower than that of the substrate Ge. The XRD theta-2theta pattern showed that the LPE Ge is strain free, while the substrate Ge is strained due to the lattice mismatch between Ge and CeO_2 . The strain relaxation leads to more defects in the substrate Ge. Yet, this cannot solely explain the significant reduction in

those caused by impurities diffusing from the buffer layers and the low-angle grain boundaries. These two sources of defects are effectively limited by the unique structure of the LPE Ge shown in Figure 4. A columnar structure is revealed in the substrate Ge²⁹. The vertical grain boundaries as illustrated in Figure 4 (a) can provide fast diffusion paths for impurities in the substrate Ge. However, a large fraction of the LPE Ge grain boundaries is horizontal as displayed in Figure 4 (b). Besides, the LPE growth is carried out at a lower range of temperature than that of the substrate Ge, which reduces the opportunity for diffusion from the underlying buffer layers. Additionally, the LPE Ge has a significantly improved texture which means much less misorientation between the grains and a largely reduced volume fraction of grain boundaries compared to that

of the substrate Ge. Therefore, much fewer defects are induced by the low-angle grain boundaries in the LPE Ge.

4. Conclusion

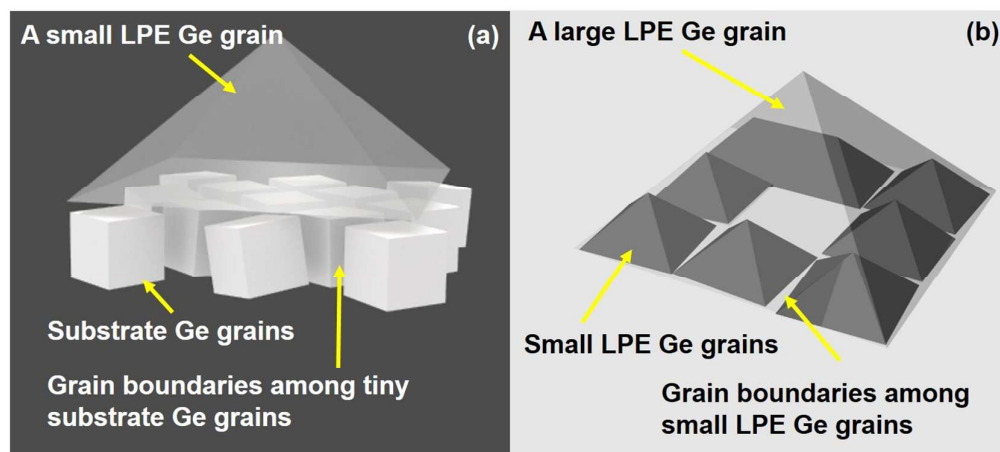


Figure 4 Basic models showing the microstructure of the LPE Ge on the substrate Ge: (a) a small LPE Ge grain on tiny substrate Ge grains, and (b) a large LPE Ge grain on small LPE Ge grains (b). The low misorientation between the grains in single-crystal-like materials is exaggerated.

In summary, device-quality Ge is achieved by an LPE method on single-crystalline-like Germanium templates over low-cost, flexible metal substrates. Defect reduction by the LPE method is found with respect to three different defect sources. The LPE Ge layer is composed of large faceted grains with size of $\sim 26 \mu\text{m}$ compared to the small substrate Ge grains with size of $\sim 200 \text{ nm}$. This large size of the LPE Ge grains effectively reduces the volume fraction of the grain boundaries. Further, through an orientation averaging mechanism²⁷, the texture of the single-crystalline-like Ge is significantly improved, with a reduction of 39.3% in $\Delta\omega$ and 76.6% in $\Delta\phi$, respectively. Therefore, the defects caused by the low-angle grain boundaries in the substrate Ge are effectively avoided in the LPE Ge. The microstructure of the LPE grains reveal a large fraction of horizontal grain boundaries in contrast to the vertical grain boundaries in the vapor-phase-deposited Ge template. The combination of a relative low volume fraction of grain boundaries and presence of mostly horizontal grain boundaries in the LPE Ge can effectively prevent the diffusion of impurities from the buffers. Further, the LPE Ge is strain free, compared to the strained substrate Ge hetero-epitaxially grown on CeO_2 . Thus, the defects caused by strain relaxation are avoided as well in the LPE Ge. The threading dislocation density is roughly estimated to be around $\sim 5 \times 10^6 \text{ cm}^{-2}$ in the LPE Ge and $\sim 1 \times 10^{10} \text{ cm}^{-2}$ in the substrate Ge. This high-quality LPE Ge has the potential to be applied as a flexible and low-cost seed layer for various kinds of micro- and nano- scale devices. Additionally, the pyramids-like structure of the LPE Ge can provide the benefit of light-trapping in solar cells to achieve a higher External Quantum Efficiency (EQE).

Conflicts of interest

There are no conflicts to declare.

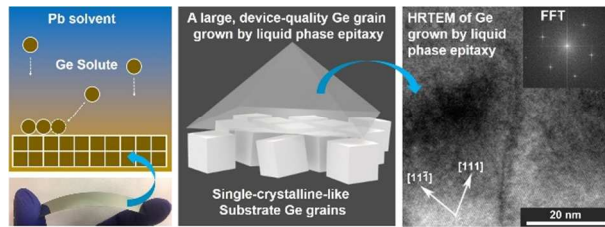
Acknowledgements

This study is supported by funding from the U. S. Department of Energy (DOE) SunShot Initiative program (Award #: DEEE0006711).

References

1. J. Bardeen and W. H. Brattain, *Physical Review*, 1948, **74**, 230.
2. W. Shockley, *Proceedings of the IRE*, 1952, **40**, 1365-1376.
3. A. Tavendale and G. Ewan, *Nuclear Instruments and Methods*, 1964, **25**, 185-187.
4. C. E. Jones, A. R. Hilton, J. B. Damrel and C. C. Helms, *Appl Optics*, 1965, **4**, 683.
5. E. E. Haller, *Materials Science in Semiconductor Processing*, 2006, **9**, 408-422.
6. D. P. Brunco, B. De Jaeger, G. Eneman, J. Mitard, G. Hellings, A. Satta, V. Terzieva, L. Souriau, F. E. Leys, G. Pourtois, M. Houssa, G. Winderickx, E. Vrancken, S. Sioncke, K. Opsomer, G. Nicholas, M. Caymax, A. Stesmans, J. Van Steenberghe, P. W. Mertens, M. Meuris and M. M. Heyns, *J. Electrochem. Soc.*, 2008, **155**, H552-H561.
7. C. O. Chui, F. Ito and K. C. Saraswat, *Ieee T Electron Dev*, 2006, **53**, 1501-1508.
8. S. Gupta, B. Magyari-Köpe, Y. Nishi and K. C. Saraswat, *J. Appl. Phys.*, 2013, **113**, 073707.
9. R. Pillarisetty, *Nature*, 2011, **479**, 324-328.
10. N. Collaert, A. Alian, H. Arimura, G. Boccardi, G. Eneman, J. Franco, T. Ivanov, D. Lin, R. Loo, C. Merckling, J. Mitard, M. A. Pourghaderi, R. Rooyackers, S. Sioncke, J. W. Sun, A. Vandooren, A. Veloso, A. Verhulst, N. Waldron, L. Witters, D. Zhou, K. Barla and A. V. Y. Thean, *Microelectronic Engineering*, 2015, **132**, 218-225.

11. D.-H. Neuhaus and A. Münzer, *Advances in OptoElectronics*, 2008, **2007**.
12. F. Dimroth, M. Grave, P. Beutel, U. Fiedeler, C. Karcher, T. N. Tibbits, E. Oliva, G. Siefer, M. Schachtner and A. Wekkeli, *Progress in Photovoltaics: Research and Applications*, 2014, **22**, 277-282.
13. V. Selvamanickam, S. Sambandam, A. Sundaram, S. Lee, A. Rar, X. Xiong, A. Alemu, C. Boney and A. Freundlich, *Journal of Crystal Growth*, 2009, **311**, 4553-4557.
14. Y. Gao, M. Asadirad, Y. Yao, P. Dutta, E. Galstyan, S. Shervin, K.-H. Lee, S. Pouladi, S. Sun and Y. Li, *Acs Appl Mater Inter*, 2016, **8**, 29565-29572.
15. Y. Gao, P. Dutta, M. Rathi, Y. Yao, M. Iliev, J.-H. Ryou and V. Selvamanickam, 2014. *Photovoltaic Specialist Conference (PVSC), 2014 IEEE 40th*, 2014, 1287-1291.
16. P. Dutta, M. Rathi, N. Zheng, Y. Gao, Y. Yao, J. Martinez, P. Ahrenkiel and V. Selvamanickam, *Applied Physics Letters*, 2014, **105**, 092104.
17. P. Dutta, M. Rathi, Y. Yao, Y. Gao, G. Majkic, M. Iliev, J. Martinez, B. Holzapfel and V. Selvamanickam, *Rsc Advances*, 2014, **4**, 21042-21048.
18. B. J. Baliga, *J. Electrochem. Soc.*, 1986, **133**, 5C-14C.
19. B. Ferrand, B. Chambaz and M. Couchaud, *Optical Materials*, 1999, **11**, 101-114.
20. S. Nishida, K. Nakagawa, M. Iwane, Y. Iwasaki, N. Ukiyo, M. Mizutani and T. Shoji, *Solar energy materials and solar cells*, 2001, **65**, 525-532.
21. R. Olesinski and G. Abbaschian, *Journal of Phase Equilibria*, 1984, **5**, 374-377.
22. P. Campbell and M. A. Green, *Solar Energy Materials and Solar Cells*, 2001, **65**, 369-375.
23. G. Li, H. Li, J. Y. Ho, M. Wong and H. S. Kwok, *Nano letters*, 2014, **14**, 2563-2568.
24. A. J. Labelle, S. M. Thon, S. Masala, M. M. Adachi, H. Dong, M. Farahani, A. H. Ip, A. Fratlocchi and E. H. Sargent, *Nano letters*, 2015, **15**, 1101-1108.
25. A. Stekolnikov, J. Furthmüller and F. Bechstedt, *Phys. Rev. B*, 2002, **65**, 115318.
26. J. Michel, J. Liu and L. C. Kimerling, *Nature Photonics*, 2010, **4**, 527-534.
27. S. Gsell, M. Schreck, R. Brescia, B. Stritzker, P. N. Arendt and J. R. Groves, *Jpn J Appl Phys*, 2008, **47**, 8925-8927.
28. J. S. Speck, M. A. Brewer, G. Beltz, A. E. Romanov and W. Pompe, *J. Appl. Phys.*, 1996, **80**, 3808-3816.
29. M. Rathi, P. Dutta, N. Zheng, Y. Yao, D. Khatiwada, A. Khadimallah, Y. Gao, S. Sun, Y. Li, S. Pouladi, P. Ahrenkiel, J. H. Ryou and V. Selvamanickam, *Journal of Materials Chemistry C*, 2017, **5**, 7919-7926.



Device-quality germanium is achieved using liquid phase epitaxy on single-crystalline-like germanium templates based on low-cost, flexible metal tapes.